Numerical Study on Structural Integrity of Inner Barrel Caused by Thermal Stratification in Upper Plenum of Monju

Atsushi Kodama, Takashi Takata, Akira Yamaguchi
Osaka University
2-1 Yamada-oka, Suita, Osaka, 5650871, Japan
kodama_a@qe.see.eng.osaka-u.ac.jp, takata_t@see.eng.osaka-u.ac.jp,
yamaguchi@see.eng.osaka-u.ac.jp

ABSTRACT

In Japanese prototype fast reactor, Monju, an inner cylinder with several flow holes is placed at the upper plenum adjacent to the core outlet. Liquid sodium heated at the core goes into the upper plenum and flows out to the hot leg piping by overflowing at the top of the inner cylinder and passing through the flow holes. When the reactor scram occurs, a cold coolant flows into the bottom of the upper plenum and the thermal stratification takes place at the upper plenum. And thus, the inner barrel may be damaged by a thermal stress due to the temperature difference of the stratification. In this study, a structural integrity of the inner barrel is evaluated numerically based on the cumulative damage rule. First, the upper plenum of fast reactor is numerically investigated to obtain the time history of the temperature at the inner barrel based on a three dimensional thermal-hydraulic CFD tool (FLUENT code) based on the IAEA benchmark analysis (Reactor scram from 40% power operation).Then, a thermal stresses at each location of the inner barrel is calculated using the time history. With regard to the thermal stress calculation, a simplified model is assumed in which temperature decay due to heat convection through the barrel and heat conduction inside the barrel and heat contraction due to temperature difference caused by the stratification are considered. In addition, a model is combined with the effects of transient heat conduction. Then a cumulative damage factor is obtained at each computational cell of the barrel and is summed up through the stratification phenomenon. It is concluded that no significant cumulative damage is found during the IAEA benchmark condition. It is also notified that a practical damage assessment can be examined numerically using the present method.

KEYWORDS

Thermal stratification, Structural integrity, Monju, Upper plenum

1. INTRODUCTION

In a sodium cooled fast reactor, high temperature and large temperature difference of the coolant can be achieved due to its high boiling point comparing with that in a light water reactor. Also thermal conductivity of liquid sodium is quite high and structure temperature is much affected by the coolant. Accordingly, thermal stress will be a significant factor of mechanical damage. Therefore, a structural analysis coupled with a thermal-hydraulics phenomenon is important problem.

Figure 1 shows an upper plenum structure in Japanese prototype fast breed reactor, Monju. [1] A schematic of temperature distribution after a reactor scram is also pictured in Fig. 1. Black lines indicate an inner barrel allocated in the upper plenum that suppresses a direct flow to the

plenum outlet and enhances a temperature mixing at the upper plenum.

When the reactor scram occurs, a core power decreases rapidly and thus a cold coolant flows out at the bottom of the upper plenum from the core outlet as shown in Fig. 1. On the other hand, the coolant of high temperature remains at the upper plenum because of rapid decrease of coolant flow rate. Hence the cold coolant stays at a bottom side and the hot coolant flows out gradually from the upper plenum. As a result, a thermal stratification takes place at the upper plenum.

Since high temperature gradient due to the stratification affects the inner barrel directly, it might be damaged caused by thermal stress. Additionally, the stratification doesn't disappear until the cold coolant reaches top of the inner barrel and it will be damaged for a long time especially under a natural circulation heat removal condition.

A turbine scram test from 40% power output conditions was conducted by Japan Nuclear Cycle (JNC, predecessor of Japan Atomic Energy Agency) in December 1995 and was well summarized as a benchmark analysis. [2]

From the viewpoint of structural integrity caused by thermal stress, a coupling of thermal-hydraulics simulation and structure analysis is useful. However, a detail coupling of them requires much computational cost. As for a thermal stress analysis for the thermal stratification, a simplified model has been proposed to use for designing. [3] However a steady state temperature distribution is taken into account in the existing model and no bending stresses caused by temperature distribution across a wall thickness.

In this study, a modification of thermal stress analysis model has been carried out in which time history of the temperature distribution in taken into consideration as well as the bending stress. Furthermore, the structural integrity of the inner barrel is evaluated numerically based on the cumulative damage rule by using the computational result of the thermal-hydraulics analysis.

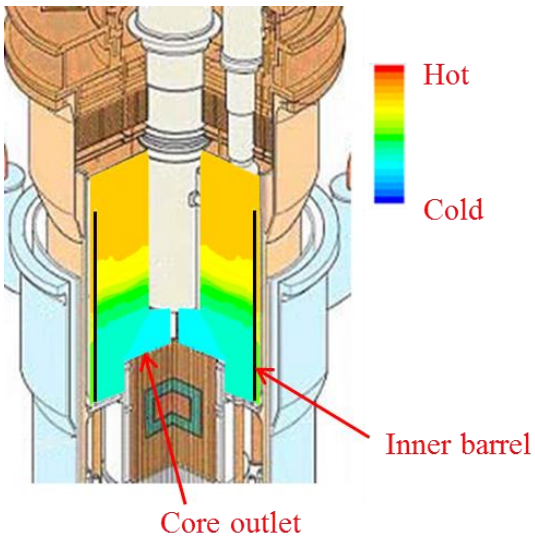

Fig. 1 Upper plenum of Monju [1]

2. THERMAL-HYDRAULICS ANALYSIS

2.1. ANALYTICAL CONDITION

A three dimensional thermal-hydraulics analysis is conducted to simulate a turbine scram test by JNC. The report of a benchmark analysis [2] consist the major features of Monju, conditions of a turbine scram test, the geometry of the upper plenum of Monju and boundary conditions of a coolant from core outlet. Various conditions and figures of thermal-hydraulics analysis are set by data of the report.

Numerical analysis by using a CFD tool, FLUENT, obtain the temperature of a coolant in the upper plenum of Monju. The analytical region is the area which coolant is flowing and an outlet piping in the upper plenum. The one-sixth model of the upper plenum is used to shorten computational cost.

The core outlet is defined the inflow conditions and the outlet of the upper plenum is defined the outflow conditions based on the benchmark analysis. The inflow conditions are given to each flow channel as the flow rate and the temperature. The boundary of the upper core structure, a side of the upper plenum, the lower plenum and the free liquid level are defined adiabatic conditions. Initial conditions as before the reactor scram are results of steady state analysis with the inflow conditions at 0 s.

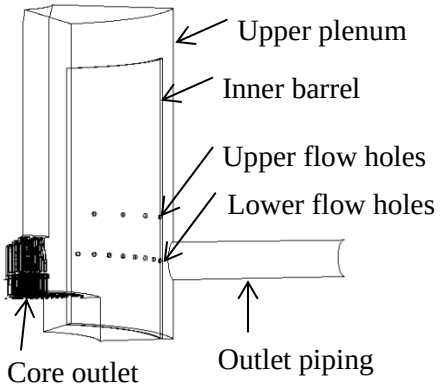

Fig. 2 Analytical region of Monju

2.2. RESULTS AND DISCUSSION

Figure 3 shows the axial temperature distribution in results and a benchmark analysis at a TC-plug during 7200 s. The position of 0 mm indicates a liquid level. A dash line at -4380 mm indicates the position of upper flow holes which pass a coolant. Also solid line at -5300 mm indicates position of lower flow holes. Additionally, the inner barrel is allocated between -1050 mm to -6930 mm.

Temperature gradient stays for a long time as seen in Fig. 3, and thermal stress may occur for a long time. Results of analysis are roughly consistent with the benchmark analysis except above the top of the inner barrel. This difference may be caused by large agitation of a coolant in the area above the inner barrel. However, it has little impact on the structural integrity because the inner barrel is evaluated thermal stress in this study.

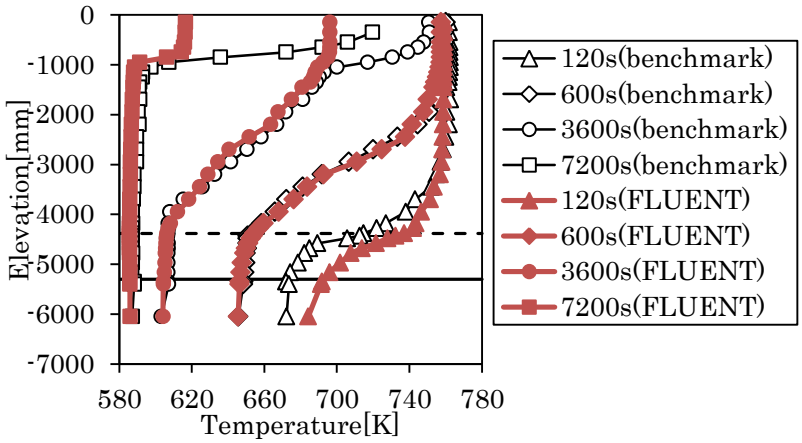

Fig. 3 Distribution of axial temperature

3. THERMAL STRESSES BY THERMAL STRATIFICATION

3.1. ANALYTICAL METHOD

A simplified method of thermal stress analysis is used to evaluate for designing. [3] However an unsteady thermal conduction and bending stress doesn't include in this method. Also detail analysis to use Finite Element Method (FEM) needs much computational cost.

Therefore the method of thermal stress analysis is modified with time history of the temperature distribution and bending stress. First, one-dimensional unsteady thermal conduction [4] is analyzed with the result of thermal-hydraulics analysis. This analysis gets the mean temperature in a wall thickness, the temperature difference across a wall thickness as a bending component of the temperature distribution and thermal stress of a non-linear component. Second, thermal stress is analyzed by axisymmetric shell theory [5] using the temperature distribution of the result of one-dimensional unsteady thermal conduction analysis.

3.1.1. ONE-DIMENSIONAL UNSTEADY THERMAL CONDUCTION

Time history of the temperature distribution causes a huge impact on unsteady thermal stress. The temperature difference across a wall thickness is especially significant in unsteady thermal stress and differs greatly from steady state analysis.

One-dimensional unsteady thermal conduction analysis is considered a wall in which heat transfer only to the thickness direction, and a side surface is defined adiabatic condition. The thickness direction is defined with x-coordinate of x=0 at external surface and x=l at internal surface. Time history of the temperature in the result of thermal hydraulics analysis is given to internal surface as boundary condition.

The evaluation of unsteady thermal conduction is described as the sum of the four problems: the first of a steady state thermal conduction problem, the second of a diffusion decay problem of unsteady component of an initial temperature, the third of a time-varying boundary condition at x=l, the fourth of a time-varying boundary condition at x=0. However the fourth problem is ignored because external surface is given adiabatic condition in this model.

The sum of each problem as the temperature distribution which is written as:

$$\boldsymbol{T(x,t) = T_s(x) + T_0(x,t) + T_2(x,t)} \quad (1)$$

Here, $T_s(x)$ is the result of a steady state thermal conduction analysis, $T_0(x)$ is unsteady component of an initial temperature, $T_2(x,t)$ is a time-varying condition at internal surface. These are evaluated from a fluid temperature and physical properties. Each temperatures and stresses get by using $T(x,t)$are given by:

$$T_H(t) = T(l,t) \quad (2)$$

$$T_M(t) = \frac{1}{l}\int_0^l T(x,t)dx \quad (3)$$

$$T_B(t) = \frac{12}{l^2}\int_0^l T(x,t)\left(x - \frac{l}{2}\right)dx \quad (4)$$

$$\sigma_H(t) = -\frac{E\alpha(T_H(t) - T_M(t))}{1-\nu} \quad (5)$$

$$\sigma_B(t) = -\frac{E\alpha T_B(t)}{2(1-\nu)} \quad (6)$$

$$\sigma_P(t) = \sigma_H(t) - \sigma_B(t) \quad (7)$$

Here, $T_H(t)$ is the temperature at internal surface, $T_M(t)$ is the mean temperature in a wall thickness, $T_B(t)$ is the temperature difference at internal and external surface as bending component, $\sigma_H(t)$ is thermal stress of internal surface, $\sigma_B(t)$ is bending stress, $\sigma_P(t)$ is the peak component of thermal stress. Furthermore, thermal stress are analyzed by axisymmetric shell theory with $T_M(t)$, $T_B(t)$ and $\sigma_P(t)$ of the result of this section.

3.1.2. SHELL SOLUTIONS OF THERMAL STRESSES

Figure 4 shows the axial temperature distribution of $T_M(t)$ and $T_B(t)$ in the result of one-dimensional unsteady thermal conduction analysis. In this section, the temperature distribution is described $T_M(z)$ and $T_B(z)$ because thermal stress are evaluated for each instant of time. Z-coordinate is defined z=0 at lower turnoff point and z=L at upper turnoff point.

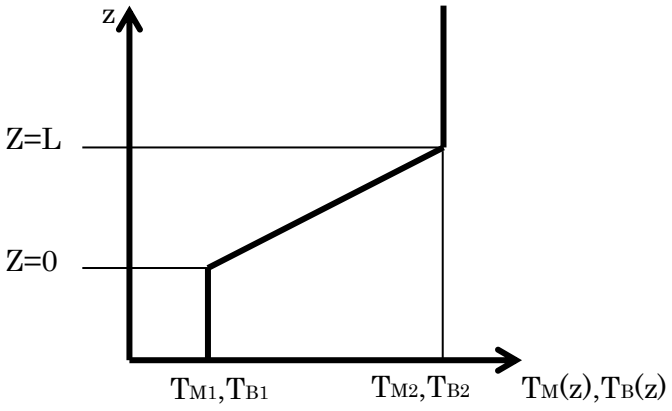

Fig. 4 Model of the axial temperature

The shell solutions by using axisymmetric shell theory get three stresses: the first of axial bending stress $\sigma_{zb}(z)$, the second of circumferential bending stress $\sigma_{hb}(z)$, the third of circumferential membrane stress $\sigma_{hm}(z)$, are written as:

$$\begin{aligned}\sigma_{zb}(z) = {} & \frac{E\alpha Rt\beta}{4(1-\nu^2)}\frac{\Delta T_M}{L}\{e^{-\beta|z|}(\cos(\beta z)+\sin(\beta|z|)) \\ & - e^{-\beta|z-L|}(\cos(\beta(z-L)+\sin(\beta|z-L|))\} \\ & + \frac{E\alpha}{8\beta(1-\nu)}\frac{\Delta T_B}{L}\{e^{-\beta|z|}(\cos(\beta z)-\sin(\beta|z|)) \\ & - e^{-\beta|z-L|}(\cos(\beta(z-L)-\sin(\beta|z-L|))\} \\ & - \frac{E\alpha T_B(z)}{2(1-\nu)} + \sigma_P \end{aligned} \tag{8}$$

$$\begin{aligned}\sigma_{hb}(z) = {} & \nu\frac{E\alpha Rt\beta}{4(1-\nu^2)}\frac{\Delta T_M}{L}\{e^{-\beta|z|}(\cos(\beta z)+\sin(\beta|z|)) \\ & - e^{-\beta|z-L|}(\cos(\beta(z-L)+\sin(\beta|z-L|))\} \\ & + \nu\frac{E\alpha}{8\beta(1-\nu)}\frac{\Delta T_B}{L}\{e^{-\beta|z|}(\cos(\beta z)-\sin(\beta|z|)) \\ & - e^{-\beta|z-L|}(\cos(\beta(z-L)-\sin(\beta|z-L|))\} \\ & - \frac{E\alpha T_B(z)}{2(1-\nu)} + \sigma_P \end{aligned} \tag{9}$$

$$\begin{aligned}\sigma_{hm}(z) = {} & \frac{E\alpha}{4\beta}\frac{\Delta T_M}{L}\{e^{-\beta|z|}(\cos(\beta z)-\sin(\beta|z|)) \\ & - e^{-\beta|z-L|}(\cos(\beta(z-L)-\sin(\beta|z-L|))\} \\ & - \frac{E\alpha(1+\nu)}{8R\beta^3 t}\frac{\Delta T_B}{L}\{e^{-\beta|z|}(\cos(\beta z)+\sin(\beta|z|)) \\ & - e^{-\beta|z-L|}(\cos(\beta(z-L))+\sin(\beta|z-L|))\} \end{aligned} \tag{10}$$

Here, E, α, R, t and ν are the Young's modulus, the coefficient of thermal expansion, the inner radius of the upper plenum and the thickness of the inner barrel of the upper plenum. $T_M(z)$, $T_B(z)$ and $\sigma_P(z)$ is the result of the previous section. $\Delta T_M = T_{M2} - T_{M1}$ and $\Delta T_B = T_{B2} - T_{B1}$ are the temperature difference of the thermal stratification in Fig. 4. β is given by:

$$\beta = \sqrt[4]{\frac{Et}{4DR^2}}, D = \frac{Et^3}{12(1-\nu^2)} \tag{11}$$

The equivalent stress, von Mises stress, is calculated as uniaxial stress by using Eq. (8), Eq. (9) and Eq. (10). The von Mises stress σ_{VM} is written as:

$$\sigma_{VM} = \sqrt{\frac{1}{2}\{\sigma_{zb}^2 + (\sigma_{hm}+\sigma_{hb})^2 + (\sigma_{hm}+\sigma_{hb}-\sigma_{zb})^2\}} \tag{12}$$

Additionally, temperature gradient is divided into an upper position and a lower position, because temperature gradient isn't constant at the section of the thermal stratification in actual phenomenon. Steep gradient and gradual gradient are given for $T_M(z)$, and positive gradient and negative gradient are given for $T_B(z)$.

3.2. BENCHMARK ANALYSIS

Two models are compared thermal stress in a modified thermal stress analysis mentioned at the previous section and a FEM tool, ANSYS. Figure 5 shows the location of the cross section of the analytical model. The cross section of a hollow cylinder is modeled as two-dimensional axisymmetric object. However the data in an axial direction of 0.5 m of top and bottom is rejected to ignore the effect of the edge, because of assumption of an infinite cylinder in a modified thermal stress analysis. The axial direction of the cross section is equally divided into 500 meshes and the thickness direction of the cross section is equally divided into 10 meshes.

Thermal-structural coupled analysis is conducted by using an element of coupled-field solid, PLANE223. The material properties are given the constant data at 700 K of SUS304 as shown in Table 1. And the heat-transfer coefficient is given by the result of thermal-hydraulics analysis. Displacement boundary conditions are freedom in all surfaces including top and bottom boundaries. Thermal boundary conditions are adiabatic except of internal surface which is given by a fluid temperature through heat convection.

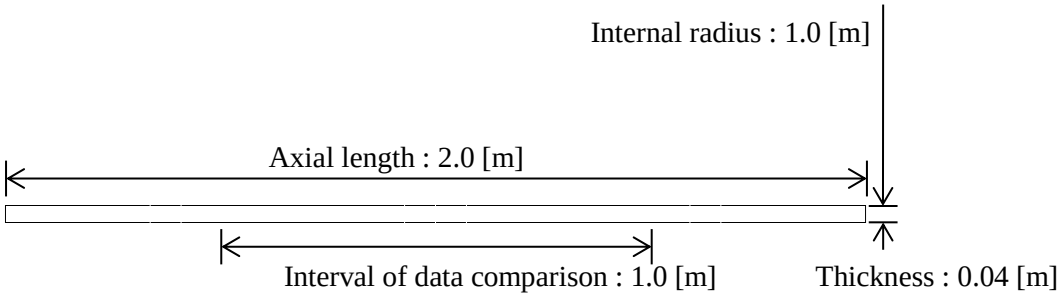

Fig. 5 Location of the analytical model

Table 1. Material properties

Young's modulus	193 [GPa]
Poisson's ratio	0.33 [-]
Density	7771.27 [kg/m^3]
Coefficient of thermal expansion	1.81e-5 [1/K]
Coefficient of thermal conductivity	20.71 [W/m/K]
Specific heat	590.05 [J/kg/K]
Heat-transfer coefficient	35000 [W/m^2/K]

Figure 6 shows the temperature distribution of the first simplified model which doesn't raise the elevation of the thermal stratification. The temperature is constant in an upper side whereas decreases of 1 K/s in a lower side. The divided temperature gradient isn't included in this model because the gradient is constant at the thermal stratification.

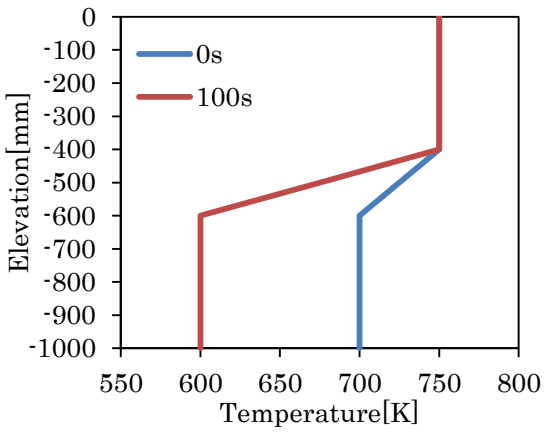

Fig. 6 Temperature distribution of the first simplified model

Figure 7 shows the von Mises stress distribution as thermal stresses of the result of the internal surface at 100 s. The maximum stress difference of the both analyses is 14.85 MPa. In other words, this difference is 4.04 % of the largest stress in FEM. The result of the modified method is in close agreement with the result of FEM.

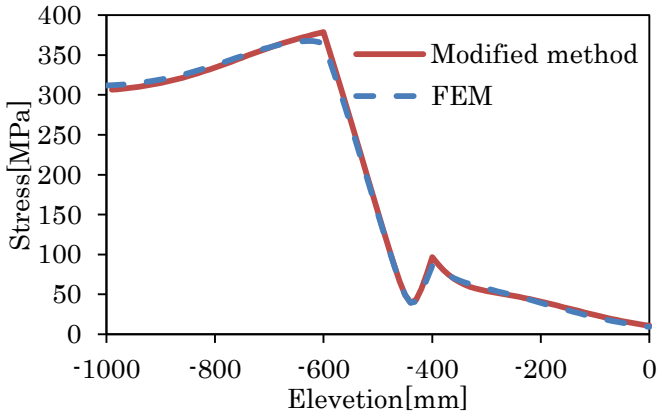

Fig. 7 Thermal stress of the first simplified model

Figure 8 shows the temperature distribution of the second simplified model which the thermal stratification raise of 4 mm/s. This simplified model includes all modified components.

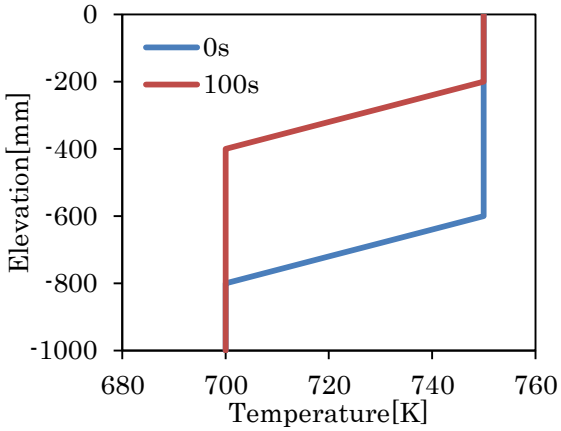

Fig. 8 Temperature distribution of the second simplified model

Figure 9 shows the von Mises stress distribution as thermal stresses of the result of the internal surface at 100 s. Fig. 9 includes the result of a previous method. [3] The maximum stress difference of FEM and a modified method is 8.14 MPa. In other words, this difference is 5.02 % of the largest stress. The result of a modified method isn't smooth stress distribution like the result of FEM. However a modified method is better than a previous method. Therefore thermal stress of actual phenomenon is evaluated by using a modified method.

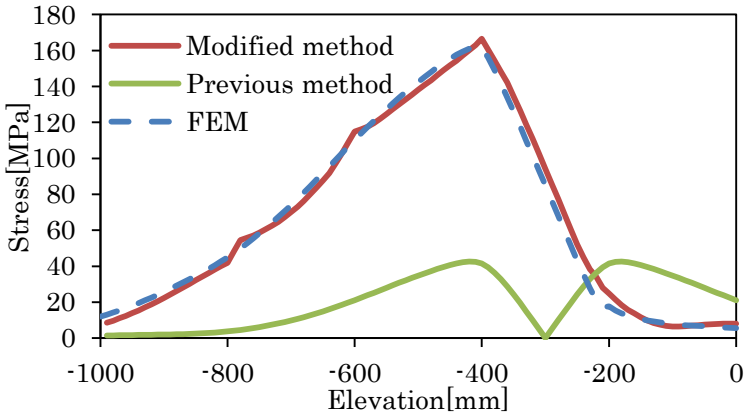

Fig. 9 Thermal stress of the second simplified model

4. STRUCTURAL INTEGRITY ASSESSMENT

4.1. THEORY OF CUMULATIVE DAMAGE

The cumulative damage as structural integrity is evaluated with time history of thermal stress. It is assumed that the inner barrel is only damaged by thermal fatigue. The operation period of reactor is defined 30 years and a reactor scram frequency is defined 1.2 times per year. [6]

The cumulative damage is calculated by using the rainflow algorithm which was proposed to evaluate fatigue damage by phenomenon of complex waves like actual operation. [7] First, complex waves are divided into the amplitude and the number of occurrences. Second, the damage per load is evaluated from the data of the stress amplitude and the number of load until fracture by fatigue test [8], S-N curve. Finally, the cumulative damage is calculated as

the sum of the damage per load, modified Miner's rule, which is written as:

$$D = \frac{n_1}{N_1} + \frac{n_2}{N_2} + \cdots + \frac{n_M}{N_M} = \sum_{i=0}^{M} \frac{n_i}{N_i} \tag{13}$$

Here, n and N are the number of load in analysis and the number of load until fracture. D is the cumulative damage that the inner barrel is indicated broken when the cumulative exceed 1.

4.2. RESULTS AND DISCUSSION

4.2.1. THERMAL STRESS OF INNER BARREL OF MONJU

Table 2 summarizes the analytical condition of thermal stress analysis by using a modified method in a previous chapter. The inner barrel is assumed that a stress concentration doesn't exist and every load is ignored except thermal stress. An analytical time is defined to 7200 s.

Table 2. Analytical condition of thermal stress analysis of Monju

Shape	Hollow cylinder
Internal radius	3.26 [m]
Thickness	0.04 [m]
Axial length	6.93 [m]

Figure 10 shows time history of the von Mises stress as thermal stress at -4000 mm in the result of a modified method, a previous method, and a previous method of which addition only unsteady thermal conduction as well as no bending stress.

The result of a modified method is smooth curve and high stress value compared to a previous method. The maximum thermal stress at all position is 213 MPa in a modified method, 69 MPa in a previous method, and 63 MPa in a method of which addition only unsteady effect. The difference between a previous method and a modified method is 144 MPa. Therefore bending stress is caused a huge thermal stress.

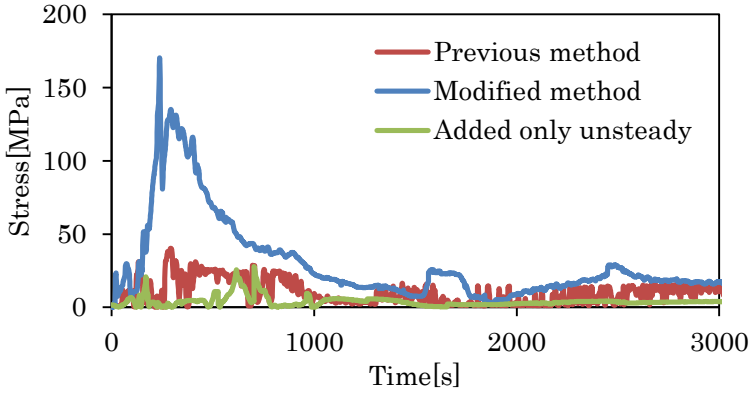

Fig. 10 Time history of thermal stress

4.2.2. CUMULATIVE DAMAGE OF INNER BARREL OF MONJU

Figure 11 shows axial distribution of the cumulative damage by using a theory of a previous section. The maximum damage is 1.56e-3 at -4160 mm where is near the position of upper flow holes at -4380 mm. The damage doesn't have a little difference except near both flow holes. In addition, the inner barrel isn't broken by thermal stress in this definition.

When the reactor scram occurs, flow rate of the coolant from core outlet rapidly decreases. Then the coolant almost flows out not through top of the inner barrel but through flow holes. Hence the temperature difference between an upper side and the flow holes gradually increases. Therefore the thermal stratification with high temperature gradient takes place near the flow holes, and stays for a long time. In consequence, the huge damage occurs near the flow holes.

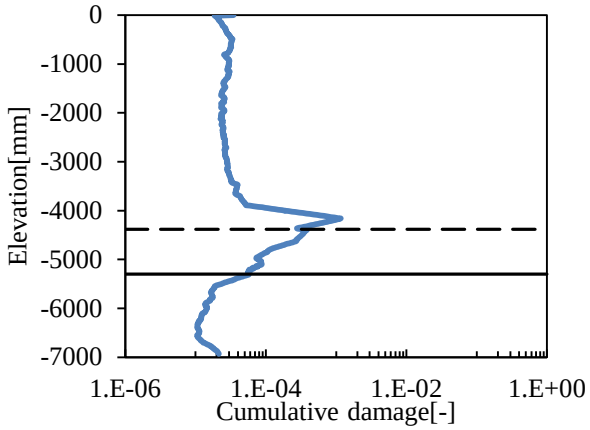

Fig. 11 Axial distribution of cumulative damage

5. CONCLUSIONS

The structural integrity of the inner barrel is needed to evaluate by a coupling of thermal-hydraulics analysis and thermal stress analysis. Therefore, the structural integrity is analyzed with three steps of thermal-hydraulics analysis, thermal stress analysis and structural integrity assessment. The temperature distribution is evaluated by thermal-hydraulics analysis by using FLUENT. The thermal-hydraulics analysis is nearly consistent except above the inner barrel with the result of a turbine scram test. The difference above the inner barrel doesn't have a large impact because thermal stress doesn't occur above the inner barrel. The thermal stress analysis is modified to combine one-dimensional thermal conduction and axisymmetric shell theory. A modified thermal stress analysis is substantially improved compared with an existing method. And a modified method agrees well with FEM. Additionally, a huge thermal stress occurs by bending stress which don't consider in an existing method. The cumulative damage is evaluated by using result of a modified thermal stress analysis. Then a result clarify that the inner barrel isn't broken by thermal stress with a condition in this study. And the impact by thermal fatigue is elucidated that the large damage occurs near the flow holes of inner barrel. This is attributed to the flow condition of a coolant is affected by existence of the flow holes.

REFERENCES

1. Sodium Technology Handbook, JNC TN9410 2005-011 (2005).
2. S. Yoshikawa, et al., "Data Description for Coordinated Research Project on Benchmark Analyses of Sodium Natural Convection in the Upper Plenum of the MUNJU Reactor Vessel", JAEA-Data/Code, 2008-024 (2009).
3. I. Furuhashi, et al., "Evaluation Charts of Thermal Stresses in Cylindrical Vessels Induced by Thermal Stratification of Contained Fluid", *Journal of computational science and technology*, **Vol.2**, pp.547-558 (2008).
4. I. Furuhashi, et al., "Development of Thermal Stress Assessment: No.5: Application to One-dimensional Transient Thermal Conduction and Varying Coefficient Problem", PNC PN9410 93-198 (1993) (in Japanese)
5. I. Furuhashi, et al., "Partitioning Design Study of Large FBR: Diagram for Thermal Stress Evaluation (Simplified Analysis of Discontinuity Thermal Stresses) ", PNC N9410 87-158 (1987)
6. M. Sotsu, et al., "Unplanned Shutdown Frequency Prediction of FBR Monju Using Fault Tree Analysis Method", *Proceeding of ICONE13*, Beijing, China, May 16-20, 2005.
7. T. Endo, et al., "Refined Rainflow Algorithm: P/V Difference Method", *Japan Society of Materials Science*, **Vol.30**, pp.89-93(1981).
8. "Databook on Fatigue Strength of Metallic Materials", The Society of Materials Science, Vol. 2, pp.853 (1982).